applied optics

Active compensation for optimal RMS wavefront error in perturbed off-axis optical telescopes using nodal aberration theory

MING WEN,[1,2,3] CHENGSHAN HAN,[1] AND HONGCAI MA[1,4]

[1]Changchun Institute of Optics, Fine Mechanics and Physics, Chinese Academy of Sciences, Changchun 130033, China
[2]University of Chinese Academy of Sciences, Beijing 100049, China
[3]e-mail: wenm602@163.com
[4]e-mail: mahc@ciomp.ac.cn

Received 10 November 2020; revised 20 January 2021; accepted 21 January 2021; posted 22 January 2021 (Doc. ID 414596); published 19 February 2021

This paper presents an active compensation strategy for RMS wavefront error of perturbed off-axis telescopes in the framework of nodal aberration theory. First, the orthogonalized expression of the wave aberration function in the vector form for perturbed off-axis telescopes is derived by using RMS normalization. The orthogonalized aberration function is applied to analytically describe the RMS wavefront error in perturbed off-axis telescopes with circular apertures. Then, the system compensation model for perturbed off-axis telescopes is established. The compensation model takes the weighted square sum of the RMS wavefront errors at representative field points as the objective function, which is minimized to obtain the optimal compensation solution of off-axis systems with perturbation constraints. The compensation model is solved by using a particle swarm optimization algorithm. Then, the off-axis three-mirror anastigmatic telescope is taken as an example, and the system compensations for the misaligned tertiary mirror and deformed primary mirror are discussed. After compensation, the average RMS wavefront errors in the perturbed off-axis systems are greatly reduced, which can well meet the system requirements. Finally, Monte Carlo simulations of the optimal compensation method and sensitivity table method are carried out to demonstrate the correctness and accuracy of the proposed method.

https://doi.org/10.1364/AO.414596

1. INTRODUCTION

To eliminate obscuration in traditional on-axis reflective telescopes with multiple mirrors, off-axis reflective telescopes have been developed [1,2], which can reduce stray light and increase optical throughput. In practical engineering, off-axis systems are increasingly used. Because of the weight constraints of space-based systems, the mirrors and supporting structures need to be lightweight, resulting in higher flexibility and lower structural frequencies. This kind of system is easily affected by severe environments such as vibration and thermal stress, which cause system aberrations and degrade the imaging capabilities. With an increase in aperture size and performance requirements, it is necessary for space-based optical systems to be equipped with active optical adjustment mechanisms to correct or compensate for system perturbations on orbit.

In a complex optical telescope, each optical element may have perturbations (component misalignments or surface deformations) that lead to degradation of image quality. In active optics [3–5], it is ideal that each optical element has the ability to correct misalignments and surface deformations, which can restore the system to the nominal state. However, it is difficult to implement in practical engineering, especially for the space-based systems with strict weight and volume constraints. To reduce system complexity and avoid using too many force actuators and adjustment devices, it is of significance for space-based optical systems to use limited adjustment devices to compensate for system performance [6,7]. For example, the effects of misalignments of larger mirrors can be compensated for by adjusting smaller mirrors; the deformation on the monolithic primary mirror (PM) can be corrected by a smaller active mirror optically conjugated to the primary [8,9].

To correct or compensate for perturbed telescopes, the corresponding adjustment values should be determined. To determine these adjustment values, several methods have been studied, such as the sensitivity table (ST) method, reverse optimization (RO) method, and a method based on nodal aberration theory (NAT). Among them, the ST method is commonly used [10]. Because the ST method basically adopts linear approximation, the accuracy is limited by the assumption. With an increase in perturbation range, the linear relationship will be broken, and the calculated adjustment values using the ST may be inaccurate. Moreover, in some optical systems, perturbation

parameters are likely to be strongly coupled, which can lead to the singularity problem in the ST method, and the calculated adjustment values can also be inaccurate. The RO method [11] uses the optimization module of optical design software to obtain adjustment values. It is easy to do on the ground, but this method is difficult to implement on orbit, except that a large number of relevant data can be continuously transmitted to the ground. Moreover, most of these methods are numerical, and so have difficulty providing deep theoretical guidance for system compensation, leading to problems in practical application. To overcome these shortcomings, the methods based on NAT are proposed.

NAT is a powerful tool for design, alignment, and analysis of nonsymmetrical systems, which was discovered by Shack [12] and developed by Thompson [13–18]. Some researches on NAT have been reported recently [19–26]. The computation strategy of misalignments and figure errors for two-mirror telescopes using NAT was presented [19]. The Large Synoptic Survey Telescope (LSST) telescope alignment plan based on NAT was reported [20]. The optical alignment of off-axis telescopes based on NAT was developed [21,22], which discussed mainly the alignment strategy for system restoration. A systematic and in-depth discussion for the aberration fields of off-axis two-mirror telescopes induced by lateral misalignment was presented [23], and some quantitative discussion on direct compensation of the effect of the PM astigmatic figure error was given. The optical compensation method for the perturbed three-mirror anastigmatic (TMA) telescope was developed, which takes the nominal aberrations as the objective for system compensation [24]. The alignment or compensation methods usually take nominal aberrations as the baseline to calculate the adjustment values. However, different from system restoration, it is not necessary for active compensation for perturbed systems to take nominal aberrations as the baseline, and it is more reasonable to aim for optimal performance of perturbed systems based on some image quality criteria. As far as we know, the analytical method of active compensation based on the optimal image quality criterion for perturbed systems is rarely involved. As a vital measure of image quality, the RMS wavefront error is often used to evaluate system performance. Therefore, in this paper, an active compensation strategy for optimal RMS wavefront error in perturbed off-axis optical telescopes based on NAT is proposed.

This paper is organized as follows. In Section 2, the wave aberration function in vector form and its orthogonalized expression for perturbed off-axis telescopes based on NAT are presented. Section 3 provides the active compensation model for perturbed off-axis telescopes. In Section 4, the verification of system compensation for an off-axis TMA telescope is demonstrated. The paper is concluded in Section 5.

2. WAVE ABERRATION FUNCTION AND ITS ORTHOGONALIZED EXPRESSION FOR PERTURBED OFF-AXIS TELESCOPES

A. Wave Aberration Function in Vector Form for Perturbed Off-Axis Systems

The wave aberration in an optical system consists of all surface contributions. The vector form of the wave aberration function in the rotationally symmetric system is given by [13]

$$W=\sum_{j}\sum_{p}^{\infty}\sum_{n}^{\infty}\sum_{m}^{\infty}W_{klmj}(\vec{H}\cdot\vec{H})^{p}(\vec{\rho}\cdot\vec{\rho})^{n}(\vec{H}\cdot\vec{\rho})^{m}, \tag{1}$$

where $k=2p+m$, $l=2n+m$, $\vec{H}$ denotes the normalized field vector, $\vec{\rho}$ is the normalized pupil vector, and W_{klmj} denotes the aberration coefficient of surface j.

The off-axis system in this paper can be considered as the off-axis portion of a rotationally symmetric on-axis system. The transformation relationship between the parent pupil vector and the decentered pupil vector is shown in Fig. 1, which can be expressed as

$$\vec{\rho}'=B\vec{\rho}+\vec{L}, \tag{2}$$

where B denotes the ratio of the radius of the decentered pupil to that of the parent pupil, $\vec{\rho}'$ and $\vec{\rho}$ designate the normalized pupil vectors of the parent system and the decentered system, respectively, and $\vec{L}$ denotes the pupil decenter vector normalized by the pupil radius of the parent system.

To develop a mathematical expression of the aberration field for a misaligned system, an effective field vector was introduced [27]. The effective aberration field height associated with the jth surface is written as

$$\vec{H}_{Aj}=\vec{H}-\vec{\sigma}_{j}, \tag{3}$$

where $\vec{\sigma}_{j}$ denotes the aberration field decenter vector for surface j, which is related directly to the corresponding misalignment parameters.

In the presence of misalignment, the wave aberration in off-axis optical systems in vector form can be expressed as

$$W=\sum_{j}\sum_{p}^{\infty}\sum_{n}^{\infty}\sum_{m}^{\infty}(W_{klm})_{j}(\vec{H}_{Aj}\cdot\vec{H}_{Aj})^{p}\times[(B\vec{\rho}+\vec{L})\cdot(B\vec{\rho}+\vec{L})]^{n}[\vec{H}_{Aj}\cdot(B\vec{\rho}+\vec{L})]^{m}. \tag{4}$$

Equation (4) can be expanded through fifth order using the rules of vector multiplication, which is the basis for NAT. Then by merging similar items, it is given by

$$W=\begin{bmatrix}\vec{\Pi}_{60}\cdot(\vec{\rho}\cdot\vec{\rho})^{3}+\vec{\Pi}_{40}\cdot(\vec{\rho}\cdot\vec{\rho})^{2}+\vec{\Pi}_{51}\cdot\vec{\rho}(\vec{\rho}\cdot\vec{\rho})^{2}\\+\vec{\Pi}_{42}\cdot\vec{\rho}^{2}(\vec{\rho}\cdot\vec{\rho})+\vec{\Pi}_{33}\cdot\vec{\rho}^{3}+\vec{\Pi}_{31}\cdot\vec{\rho}(\vec{\rho}\cdot\vec{\rho})\\+\vec{\Pi}_{22}\cdot\vec{\rho}^{2}+\vec{\Pi}_{20}\cdot(\vec{\rho}\cdot\vec{\rho})+\vec{\Pi}_{11}\cdot\vec{\rho}\end{bmatrix}, \tag{5}$$

where the notations ($\vec{\Pi}_{60}$, $\vec{\Pi}_{22}$, etc.) denote the corresponding coefficients, and where

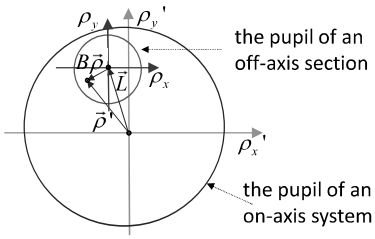

Fig. 1. Representation of relationship between the parent pupil and decentered pupil.

$$\begin{cases}
\vec{\Pi}_{22} = B^2(\vec{\Psi}_{131}+\vec{\Psi}_{331M})\vec{L}+\frac{1}{2}B^2(\vec{\Psi}^2_{222}+\vec{\Psi}^2_{422}) \\
\qquad +6W_{060}B^2(\vec{L}\cdot\vec{L})\vec{L}^2+2B^2(\vec{L}\cdot\vec{L})\vec{L}\vec{\Psi}_{151}+2B^2(\vec{\Psi}_{151}\cdot\vec{L})\vec{L}^2 \\
\qquad +2B^2(W_{040}+\Psi_{240M})\vec{L}^2+\frac{3}{2}B^2(\vec{L}\cdot\vec{L})\vec{\Psi}^2_{242}+\frac{3}{4}B^2\vec{\Psi}^3_{333}\vec{L}^*, \\
\vec{\Pi}_{31} = B^3(\vec{\Psi}_{131}+\vec{\Psi}_{331M})+4B^3(W_{040}+\Psi_{240M})\vec{L}+\frac{3}{2}B^3\vec{\Psi}^2_{242}\vec{L}^* \\
\qquad +18W_{060}B^3(\vec{L}\cdot\vec{L})\vec{L}+6B^3(\vec{L}\cdot\vec{L})\vec{\Psi}_{151}+3B^3(\vec{\Psi}_{151})^*\vec{L}^2, \\
\vec{\Pi}_{42} = 6W_{060}B^4\vec{L}^2+2B^4\vec{\Psi}_{151}\vec{L}+\frac{1}{2}B^4\vec{\Psi}^2_{242}, \\
\vec{\Pi}_{60} = B^6W_{060}, \\
\vec{\Pi}_{40} = B^4(W_{040}+\Psi_{240M})+9W_{060}B^4(\vec{L}\cdot\vec{L})+3B^4(\vec{\Psi}_{151}\cdot\vec{L}), \\
\vec{\Pi}_{51} = 6W_{060}B^5\vec{L}+B^5\vec{\Psi}_{151}, \\
\vec{\Pi}_{33} = 2W_{060}B^3\vec{L}^3+B^3\vec{\Psi}_{151}\vec{L}^2+\frac{1}{2}B^3\vec{\Psi}^2_{242}\vec{L}+\frac{1}{4}B^3\vec{\Psi}^3_{333},
\end{cases} \tag{6}$$

where the definitions of the notations ($\vec{\Psi}_{131}$, $\vec{\Psi}^2_{222}$, etc.), as defined in Ref. [28], are given in Appendix A.

It can be seen that the wave aberration in misaligned off-axis systems is the function of the aberration field decenter vectors. The coefficient expressions of the two lowest-order aperture terms are not given, as they do not contribute to image blur.

B. Orthogonalized Expression of Wave Aberration Function in Vector Form for Perturbed Off-Axis Systems

If the wave aberration function is not orthogonal, this means that the magnitude of each term depends on the other terms in system analysis. Once a proper orthogonal relationship is established, the cross terms in the aberration function can be eliminated. It greatly facilitates the subsequent analysis and processing. The orthogonal form can define a balance among classical aberrations, and the coefficients of orthogonal polynomials are independent of the number of polynomials used in the expansion. Because of the orthogonality over the unit circle, Zernike polynomials are particularly attractive in wavefront analysis. There exist several definitions of Zernike polynomials. In this paper, the convention outlined in Noll [29] is used, which uses RMS normalization.

The aberration function of a system without rotational symmetry can be expanded in terms of a set of RMS normalized Zernike polynomials [29], which can be given by

$$W(\rho,\phi) = \sum_{n=0}^{\infty}\sqrt{n+1}A_{n0}R^0_n + \sum_{n=1}^{\infty}\sum_{m=1}^{n}\sqrt{2(n+1)} \times [A_{nm}R^m_n(\rho)\cos m\phi + B_{nm}R^m_n(\rho)\sin m\phi], \tag{7}$$

where ρ and ϕ denote the radial and azimuthal components of $\vec{\rho}$, respectively, and where A_{nm} and B_{nm} are the Zernike coefficients of the corresponding terms; the radial dependence of the Zernike polynomials is expressed as

$$R^m_n(\rho) = \sum_{s=0}^{(n-m)/2}\frac{(-1)^s(n-s)!}{s!\left(\frac{n+m}{2}-s\right)!\left(\frac{n-m}{2}-s\right)!}\rho^{n-2s}, \tag{8}$$

where n and m in Eq. (7) and Eq. (8) are positive integers (including zero) known as the radial degree and the azimuthal frequency, respectively. It should be noted that $n-m\geq 0$, and $n-m$ must be an even number.

To make the Zernike description related directly to the NAT expression, the wave aberration function can be expanded over the Zernike vector, which is given by

$$W(\vec{\rho}) = \sum_{n=0}^{\infty}\sum_{m=0}^{n}\vec{C}_{nm}\cdot\vec{Z}^m_n(\vec{\rho}), \tag{9}$$

where $\vec{Z}^m_n(\vec{\rho})$ is a Zernike vector, which can be expressed as

$$\vec{Z}^m_n(\vec{\rho}) = \sqrt{\frac{2(n+1)}{1+\delta_{m,0}}}\sum_{s=0}^{(n-m)/2}\times\frac{(-1)^s(n-s)!}{s!\left(\frac{n+m}{2}-s\right)!\left(\frac{n-m}{2}-s\right)!}(\vec{\rho}\cdot\vec{\rho})^{\frac{n-m-2s}{2}}\vec{\rho}^m, \tag{10}$$

where $\delta_{m,0}$ is the Kronecker delta function ($\delta_{m,0}=0$ if $m\neq 0$; $\delta_{m,0}=1$ if $m=0$), and $\vec{C}_{nm}$ denotes the coefficient vector of the corresponding term. When $m=0$, the terms in Eq. (10) are scalars, not vectors, but scalars can also be considered as a special form of vectors, which are a useful extension to a unified vector description. Here, in accordance with the tradition of optical testing, the x axis is chosen as the reference axis [30], and the angle is measured counterclockwise from it.

According to Eq. (10), the wave aberration function expanded through fifth order in perturbed off-axis systems, in Eq. (5), can be rewritten as

$$W=\left\{\begin{array}{l}\vec{\Pi}_{22}\cdot\frac{1}{\sqrt{6}}\vec{Z}_2^2(\vec{\rho})+\vec{\Pi}_{31}\cdot\left[\frac{1}{3\sqrt{8}}\vec{Z}_3^1(\vec{\rho})+\frac{1}{3}\vec{Z}_1^1(\vec{\rho})\right]\\+\vec{\Pi}_{40}\cdot\left[\frac{1}{6\sqrt{5}}\vec{Z}_4^0(\vec{\rho})+\frac{1}{2\sqrt{3}}\vec{Z}_2^0(\vec{\rho})+\frac{1}{3}\vec{Z}_0^0(\vec{\rho})\right]\\+\vec{\Pi}_{51}\cdot\left[\frac{1}{20\sqrt{3}}\vec{Z}_5^1(\vec{\rho})+\frac{1}{5\sqrt{2}}\vec{Z}_3^1(\vec{\rho})+\frac{1}{4}\vec{Z}_1^1(\vec{\rho})\right]\\+\vec{\Pi}_{33}\cdot\frac{1}{\sqrt{8}}\vec{Z}_3^3(\vec{\rho})+\vec{\Pi}_{42}\cdot\left[\frac{1}{4\sqrt{10}}\vec{Z}_4^2(\vec{\rho})+\frac{3}{4\sqrt{6}}\vec{Z}_2^2(\vec{\rho})\right]\\+\vec{\Pi}_{60}\cdot\left[\frac{1}{20\sqrt{7}}\vec{Z}_6^0(\vec{\rho})+\frac{1}{4\sqrt{5}}\vec{Z}_4^0(\vec{\rho})+\frac{9}{20\sqrt{3}}\vec{Z}_2^0(\vec{\rho})+\frac{1}{4}\vec{Z}_0^0(\vec{\rho})\right]\\+\vec{\Pi}_{20}\cdot\left[\frac{1}{2\sqrt{3}}\vec{Z}_2^0(\vec{\rho})+\frac{1}{2}\vec{Z}_0^0(\vec{\rho})\right]+\vec{\Pi}_{11}\cdot\frac{1}{2}\vec{Z}_1^1(\vec{\rho})\end{array}\right\}. \tag{11}$$

After merging the similar items in Eq. (11), the wave aberration function can be converted into the orthogonal polynomials

$$W=\left\{\begin{array}{l}\left(\frac{1}{\sqrt{6}}\vec{\Pi}_{22}+\frac{3}{4\sqrt{6}}\vec{\Pi}_{42}\right)\cdot\vec{Z}_2^2(\vec{\rho})+\frac{1}{\sqrt{8}}\vec{\Pi}_{33}\cdot\vec{Z}_3^3(\vec{\rho})\\+\left(\frac{1}{3\sqrt{8}}\vec{\Pi}_{31}+\frac{1}{5\sqrt{2}}\vec{\Pi}_{51}\right)\cdot\vec{Z}_3^1(\vec{\rho})+\left(\frac{1}{4\sqrt{10}}\vec{\Pi}_{42}\right)\cdot\vec{Z}_4^2(\vec{\rho})\\+\left(\frac{1}{6\sqrt{5}}\vec{\Pi}_{40}+\frac{1}{4\sqrt{5}}\vec{\Pi}_{60}\right)\cdot\vec{Z}_4^0(\vec{\rho})+\left(\frac{1}{20\sqrt{3}}\vec{\Pi}_{51}\right)\cdot\vec{Z}_5^1(\vec{\rho})\\+\left(\frac{1}{20\sqrt{7}}\vec{\Pi}_{60}\right)\cdot\vec{Z}_6^0(\vec{\rho})+\left(\frac{1}{4}\vec{\Pi}_{51}+\frac{1}{3}\vec{\Pi}_{31}+\frac{1}{2}\vec{\Pi}_{11}\right)\cdot\vec{Z}_1^1(\vec{\rho})\\+\left(\frac{9}{20\sqrt{3}}\vec{\Pi}_{60}+\frac{1}{2\sqrt{3}}\vec{\Pi}_{40}+\frac{1}{2\sqrt{3}}\vec{\Pi}_{20}\right)\cdot\vec{Z}_2^0(\vec{\rho})\end{array}\right\}. \tag{12}$$

The polynomials are related to classical aberrations and provide a convenient aberration description. For the sake of orthogonality, the higher-order terms are combined with the appropriate lower-order terms. This is reasonable in view of the conventional aberration balance. The orthogonal aberration expansion presented here can be used to describe perturbed off-axis telescopes, and it is useful while trying to compensate for the performance of perturbed systems.

3. OPTIMAL SYSTEM COMPENSATION FOR RMS WAVEFRONT ERROR IN PERTURBED OFF-AXIS TELESCOPES

As an optical system becomes more and more complex, the system compensation becomes more and more challenging. Obviously, if the position and surface shape of each optical element in the system can be adjusted arbitrarily, the system can restore to the nominal state. But in engineering, due to the limitation of weight and volume, it is hoped that the system performance can be compensated for as easily as possible. The misalignments and low frequency surface errors of optical components can induce the same type of aberrations, and it is possible to balance these induced aberrations. When some perturbed components cannot be changed, it is possible to compensate for the corresponding induced aberrations by adjusting other components with motion mechanisms. This can eliminate or partially eliminate the influence of perturbations and improve system performance. In this paper, the aim of system compensation is to improve the image quality and meet the required system performance. It is more reasonable to optimize the system performance based on some image quality criteria.

Image quality can be defined in terms of RMS wavefront error, spot size, or some other quantities at the representative field points. During active optical compensation, a comprehensive image quality criterion with direct physical significance is beneficial. The RMS wavefront error is a measure of how much the wavefront surface deviates from a spherical surface. In general, RMS wavefront error is a good criterion for aberration balance. Therefore, it will be used as the measure of image quality to compensate for system performance.

A. Analytical Expression of RMS Wavefront Error for Perturbed Off-Axis Telescopes

Once the orthogonal aberration expansion for perturbed off-axis systems is developed, it can be used to calculate the image quality criterion. In this section, the RMS wavefront error with the mean subtracted is used as the measure of image quality. The wavefront variance of the fit over the circular aperture can be defined as

$$\omega^2=\frac{1}{\pi}\iint[W(\rho,\theta)]^2\rho\mathrm{d}\rho\mathrm{d}\theta-\frac{1}{\pi^2}\left[\iint W(\rho,\theta)\rho\mathrm{d}\rho\mathrm{d}\theta\right]^2, \tag{13}$$

where ω^2 is the wavefront variance. By substituting the aberration expansion of Eq. (12) into Eq. (13), the RMS wavefront error in perturbed off-axis telescopes can be expressed analytically as

$$\begin{aligned}\omega_{\mathrm{rms}}&=(\omega^2)^{\frac{1}{2}}\\&=\left\{\begin{array}{l}\left|\frac{1}{\sqrt{6}}\vec{\Pi}_{22}+\frac{3}{4\sqrt{6}}\vec{\Pi}_{42}\right|^2+\left|\frac{1}{3\sqrt{8}}\vec{\Pi}_{31}+\frac{1}{5\sqrt{2}}\vec{\Pi}_{51}\right|^2\\+\left|\frac{1}{6\sqrt{5}}\vec{\Pi}_{40}+\frac{1}{4\sqrt{5}}\vec{\Pi}_{60}\right|^2+\left|\frac{1}{\sqrt{8}}\vec{\Pi}_{33}\right|^2+\left|\frac{1}{4\sqrt{10}}\vec{\Pi}_{42}\right|^2\\+\left|\frac{1}{20\sqrt{3}}\vec{\Pi}_{51}\right|^2+\left|\frac{1}{20\sqrt{7}}\vec{\Pi}_{60}\right|^2+\Delta\end{array}\right\}^{\frac{1}{2}},\end{aligned} \tag{14}$$

where $|\cdot|$ indicates the operation of taking the module for a vector, and Δ denotes the lower-order terms, which will be treated separately.

It can be seen that the sum of the squares of the coefficients of Eq. (12) yields the wavefront variance in perturbed off-axis telescopes. The property of orthogonalization allows individual terms to be added or subtracted to the polynomials without changing the other coefficients. It allows the terms that can be corrected separately such as focus to be removed from the polynomials without affecting other terms. As the image plane can be adjusted, it does not cause any image degradation. The terms that do not affect the point image quality are not usually considered in the calculation of image quality.

The figure errors of optical components can be introduced into NAT [31], so they can also be introduced into the above image quality criterion. The RMS wavefront error can be regarded as the function of misalignments and figure errors, which provides a description of the effect of perturbations on image quality. Based on the criteria, the system compensation model can be established.

B. Optimal Compensation Model for RMS Wavefront Error in Perturbed Off-Axis Telescopes

In system compensation for off-axis optical telescopes, all the RMS wavefront errors at the representative field points need to be considered. The compensation problem is defined as

$$\begin{cases} \min[\omega_{\mathrm{rms},1}(X), \omega_{\mathrm{rms},2}(X), \cdots, \omega_{\mathrm{rms},j}(X), \cdots, \omega_{\mathrm{rms},N}(X)], \\ j = 1, 2, \cdots, N, \\ \text{s.t.} \quad X \in D, \end{cases} \tag{15}$$

where $X = (X_1, X_2 \cdots X_M)^T$ denotes the decision variables (compensation variables or their functions), M is the number of decision variables, N is the number of representative field points, $X \in D$ denotes the decision space, and $\omega_{\mathrm{rms},j}(X)$ represents the RMS wavefront error at the jth field point, which is given in Eq. (14). Assuming that the optimal value of RMS wavefront error of the jth field point is $\omega^*_{\mathrm{rms},j}$, then $\omega^*_{\mathrm{rms}} = (\omega^*_{\mathrm{rms},1}, \omega^*_{\mathrm{rms},2} \cdots \omega^*_{\mathrm{rms},N})^T$ is the ideal solution to the compensation problem. But it is difficult to achieve in the compensation model, so we can seek the satisfactory solution based only on the corresponding performance criterion.

It can be seen that it is a multi-objective optimization problem. To solve this problem, a trade-off consideration is required. To comprehensively consider the image quality of the whole field of view (FOV), the weighted square sum of RMS wavefront errors at representative field points is used as the objective function. The optimal compensation model for perturbed off-axis telescopes may be stated as follows:

$$\begin{cases} \min \sum_{j=1}^{N} \lambda_j [\omega_{\mathrm{rms},j}(X)]^2, \\ \text{s.t.} \quad X \in D, \end{cases} \tag{16}$$

where λ_j is the field weighting factor, which represents the importance of the corresponding field point. The general compensation model for RMS wavefront error in perturbed off-axis telescopes is established.

It should be noted that compensating for perturbations with other perturbations usually leads to an inclination of the beam with respect to the optical axis of the PM, and requiring focus and tilt adjustments of the focal plane (FP). To solve the optimal model conveniently, the focus term is treated separately. By solving the compensation model, the optimal compensation values (except focus and tilt) can be determined. Then, according to the fringe Zernike coefficient for the medial focal surface at representative field points, by using the most commonly used least-squares method, the focus and tilt adjustments of FP can be easily determined.

C. Solving Method of the Compensation Model Based on Particle Swarm Optimization

The mathematical models of practical engineering problems are often difficult to solve accurately. In the above compensation model, the relationship between the objective function and the decision variables is nonlinear. When the nonlinearity of the model is strong, it is difficult to solve accurately.

In this paper, a particle swarm optimization (PSO) algorithm [32] is used to solve the compensation problem. PSO is a generic optimization method, which has the advantages of fast calculation speed, good global search ability, and fewer parameters to be adjusted, so it is used more and more in the field of function optimization.

The flow diagram of the PSO algorithm for the compensation problem is shown in Fig. 2. The process of the algorithm is described as follows.

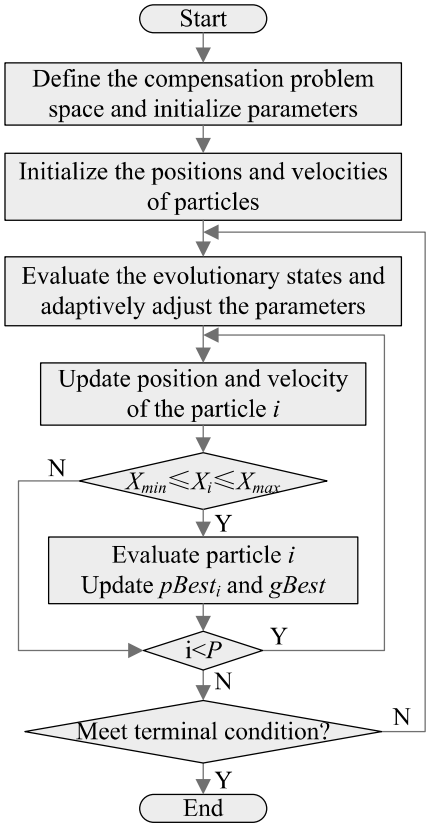

Fig. 2. Flow diagram of PSO algorithm for the compensation model.

Step 1. Define the compensation problem space and initialize parameters.

Step 2. Initialize the positions and velocities of particles (population size is P). These particle positions represent the set of compensation solutions.

Step 3. Evaluate the evolutionary states and adaptively adjust the parameters.

Step 4. Update position X_i and velocity V_i of the associated particle. The range of position is $[X_{\min}, X_{\max}]$.

Step 5. Evaluate the associated particle and update the individual best (pBest_i) and global optimal position (gBest).

Step 6. Repeat steps 3–5 until the stopping criterion is satisfied, and give the results.

The decision values of the above compensation model can be obtained by using the above steps. Of course, if the accuracy requirement is not high, the compensation model can be simplified, and then it can be solved analytically.

4. VERIFICATION OF SYSTEM COMPENSATION FOR THE PERTURBED OFF-AXIS TMA TELESCOPE

One of the most commonly used types of off-axis telescopes is the off-axis TMA system, because it has fewer optical components while maintaining good system performance. This section takes the off-axis TMA telescope as a typical example for discussion. Generally speaking, the secondary mirror (SM) of the system is much smaller than the PM and the tertiary mirror

(TM), so it is relatively easy to be adjusted in engineering. This section discusses mainly the system compensation by adjusting the SM. It is also often used in practical engineering, and it is of significance to simplify the configuration of space active optical systems. Without losing generality, two cases are considered: one to compensate for the misaligned TM by adjusting SM, and the other to compensate for the deformed PM. Other cases can be treated in a similar way.

A. Optimal System Compensation for Off-Axis TMA System with Misaligned TM

Misaligned optical components induce aberrations, and they often induce the same kind of aberrations. A misaligned system can be compensated for by balancing the misalignment-induced aberrations of different components. In this subsection, optimal compensation of the off-axis TMA system with misaligned TM by adjusting SM is discussed. The compensation model takes the decision variables to a region of solution where the induced aberrations are mutually balanced. The compensation variables considered here are the lateral misalignment of SM.

Most large optical systems have an aperture stop located on PM. So here, the stop is located on PM, which is chosen as the coordinate reference. The aberration field decenter vectors of SM and TM can be expressed as

$$\begin{cases} \vec{\sigma}_{\mathrm{TM}}^{\mathrm{sph}} = \vec{P} + 2(1 + c_{\mathrm{TM}} d_2)[(1 + c_{\mathrm{SM}} d_1)\bar{u}_{\mathrm{PM}}]\vec{\sigma}_{\mathrm{SM}}^{\mathrm{sph}}/G_S, \\ \vec{\sigma}_{\mathrm{TM}}^{\mathrm{asph}} = \vec{Q} + 2d_2(1 + c_{\mathrm{SM}} d_1)\bar{u}_{\mathrm{PM}}\vec{\sigma}_{\mathrm{SM}}^{\mathrm{sph}}/G_A, \\ \vec{\sigma}_{\mathrm{SM}}^{\mathrm{sph}} = (\vec{S} + c_{\mathrm{SM}}\vec{T})/G_M, \\ \vec{\sigma}_{\mathrm{SM}}^{\mathrm{asph}} = \vec{T}/G_P, \end{cases} \tag{17}$$

where

$$\begin{cases} \vec{P} = \dfrac{c_{\mathrm{TM}}}{G_S}\begin{bmatrix} \mathrm{XDE_{TM}} \\ \mathrm{YDE_{TM}} \end{bmatrix} + \dfrac{1}{G_S}\begin{bmatrix} -\mathrm{BDE_{TM}} \\ \mathrm{ADE_{TM}} \end{bmatrix}, \\ \vec{Q} = \dfrac{1}{G_A}\begin{bmatrix} \mathrm{XDE_{TM}} \\ \mathrm{YDE_{TM}} \end{bmatrix}, \quad \vec{S} = \begin{bmatrix} \mathrm{BDE_{SM}} \\ -\mathrm{ADE_{SM}} \end{bmatrix}, \\ \vec{T} = -\begin{bmatrix} \mathrm{XDE_{SM}} \\ \mathrm{YDE_{SM}} \end{bmatrix}, \\ G_S = [c_{\mathrm{TM}}(d_2 - d_1) + 2c_{\mathrm{SM}}(c_{\mathrm{TM}} d_1 d_2 + d_1) + 1]\bar{u}_{\mathrm{PM}}, \\ G_A = [d_2 + d_1(2c_{\mathrm{SM}} d_2 - 1)]\bar{u}_{\mathrm{PM}}, \\ G_M = (1 + c_{\mathrm{SM}} d_1)\bar{u}_{\mathrm{PM}}, \\ G_P = d_1 \bar{u}_{\mathrm{PM}}, \end{cases} \tag{18}$$

where $\vec{\sigma}_{\mathrm{SM}}^{\mathrm{sph}}$ and $\vec{\sigma}_{\mathrm{SM}}^{\mathrm{asph}}$ denote the aberration field decenter vectors for SM; $\vec{\sigma}_{\mathrm{TM}}^{\mathrm{sph}}$ and $\vec{\sigma}_{\mathrm{TM}}^{\mathrm{asph}}$ designate the aberration field decenter vectors for TM; $\mathrm{XDE_{SM}}$, $\mathrm{YDE_{SM}}$, $\mathrm{ADE_{SM}}$, and $\mathrm{BDE_{SM}}$ are the misalignments of SM; $\mathrm{XDE_{TM}}$, $\mathrm{YDE_{TM}}$, $\mathrm{ADE_{TM}}$, and $\mathrm{BDE_{TM}}$ denote the misalignments of TM; c_{SM} is the curvature of SM; c_{TM} denotes the curvature of TM; d_1 is the mirror spacing between PM and SM; d_2 is the spacing between SM and TM; $\bar{u}_{\mathrm{PM}}$ is the incidence angle of the chief ray at the PM; and superscripts *sph* and *asph* denote contributions of the spherical base and aspheric departure, respectively. For the spherical base, the relevant optical characteristic point is the location of the center of curvature of the surface. Here, XDE and YDE are the mirror vertex decenters in the x-z and y-z planes, respectively, and ADE and BDE are the mirror tip-tilts in the x-z and y-z planes, respectively.

As SM and TM are in the state of misalignment, the image quality criterion can be regarded as the function of their misalignments. According to Eq. (17), the aberration field decenter vectors of TM can be described by that of SM. Therefore, the compensation model for the off-axis TMA system with misaligned TM by adjusting SM can be expressed as

$$\begin{cases} \min \sum_{j=1}^{N} \lambda_j \left[\omega_{\mathrm{rms},j}\left(\sigma_{\mathrm{SM},x}^{\mathrm{sph}}, \sigma_{\mathrm{SM},y}^{\mathrm{sph}}, \sigma_{\mathrm{SM},x}^{\mathrm{asph}}, \sigma_{\mathrm{SM},y}^{\mathrm{asph}}\right)\right]^2, \\ \text{s.t.} \quad \left\{\sigma_{\mathrm{SM},x}^{\mathrm{sph}}, \sigma_{\mathrm{SM},y}^{\mathrm{sph}}, \sigma_{\mathrm{SM},x}^{\mathrm{asph}}, \sigma_{\mathrm{SM},y}^{\mathrm{asph}}\right\} \in (-1, 1), \end{cases} \tag{19}$$

where subscripts x and y denote the two components of the corresponding decenter vectors.

By solving the above model, the aberration field decenter vectors of SM can be obtained. According to the transformation relation of Eq. (17), the optimal compensation values of SM can be determined. After SM is adjusted, the compensation values of FP can be determined using the wavefront data at the typical field points.

The optical layout of the off-axis TMA telescope used in this section is shown in Fig. 3. It has a stop aperture diameter of 1000 mm with a 2.3° × 0.3° FOV. The radius values of PM, SM, and TM are −8004.06, −2021.03, and −2712.44, respectively. The thickness values between mirrors are −3446.93 and 3491.15, respectively. The conic values of PM, SM, and TM are −0.921, −4.717, and −0.293, respectively. To perform this example, several FOVs are selected, which are (1.15°, −0.15°), (−1.15°, −0.15°), (−1.15°, −0.45°), (1.15°, −0.45°), (0.58°, −0.2°), (−0.58°, −0.2°), (0.58°, −0.4°), (−0.58°, −0.4°), respectively. Here, the introduced misalignments of TM for the off-axis TMA telescope are shown in Table 1. In the compensation model, all weights are equal ($\lambda_j = 1$), which means that all field points are weighted equally. The search space of the aberration field decenter vectors is (−1, 1), the population size of PSO is 30, and the maximum number of iterations of PSO is 2000. Using these parameters, the aberration field decenter vectors of SM for system compensation can be determined, which are $\sigma_{\mathrm{SM},x}^{\mathrm{sph}} = -9.378 \times 10^{-4}$, $\sigma_{\mathrm{SM},y}^{\mathrm{sph}} = -1.991 \times 10^{-3}$, $\sigma_{\mathrm{SM},x}^{\mathrm{asph}} = 3.765 \times 10^{-3}$, and $\sigma_{\mathrm{SM},y}^{\mathrm{asph}} = 4.731 \times 10^{-3}$. Then, according to Eq. (17), the compensation values of SM for the off-axis TMA telescope with misaligned TM can be determined. For system compensation, the compensation values cannot be compared

Table 1. Introduced (I-M) Misalignments of TM for the Off-Axis TMA Telescope[a]

	$\mathrm{XDE_{TM}}$	$\mathrm{YDE_{TM}}$	$\mathrm{ADE_{TM}}$	$\mathrm{BDE_{TM}}$
I-M	−0.2500	0.1000	0.0200	−0.0150

[a]XDE and YDE are in millimeters, ADE and BDE in degrees.

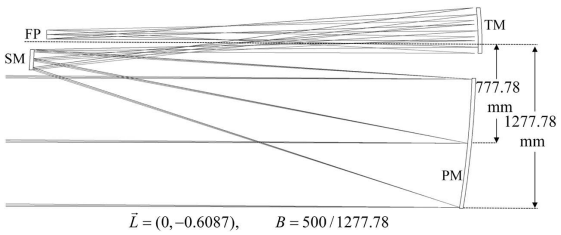

Fig. 3. Optical layout of the off-axis TMA system.

Table 2. Computed (C-V) and Referred (R-V) Compensation Values of SM and FP for the Off-Axis TMA Telescope with Misaligned TM[a]

	XDE_{SM}	YDE_{SM}	ADE_{SM}	BDE_{SM}
R-V	0.2838	0.3580	0.0167	−0.0113
C-V	0.2796	0.3515	0.0166	−0.0111
	ZDE_{FP}	ADE_{FP}	BDE_{FP}	
R-V	−0.0119	−0.0801	0.0465	
C-V	−0.0128	−0.0771	0.0466	

[a]XDE, YDE, and ZDE are in millimeters, ADE and BDE in degrees.

with the introduced misalignment values directly. To evaluate the computed compensation values based on the proposed method, the referred values need to be determined. They can be obtained by optimization processing support embedded in optical simulation software. The computed and referred compensation values of SM and FP for the misaligned TM are listed in Table 2. It can be seen that the computed compensation values are very close to the referred values.

The computed compensation values are introduced into the perturbed system in optical simulation software. Full field displays (FFDs) of RMS wavefront errors before and after compensating for the misaligned TM are shown in Fig. 4. It can be found that the RMS wavefront errors of the off-axis TMA telescope with misaligned TM can be well compensated for. The average RMS wavefront error in the off-axis system is reduced from 0.088λ (after misalignment) to 0.039λ (after compensation), which can well meet the system performance requirements (0.07 waves limit). It indicates that the proposed compensation method is correct and effective.

B. Optimal System Compensation for Off-Axis TMA System with Deformed PM

If the rigid-body motions of small optical components can compensate for typical surface deformations of large aperture components, active optical configuration of space systems can be greatly simplified. It can reduce the complexity and improve the stability of optical systems. Low frequency surface deformations and misalignments often induce the same types of aberrations, and there exist compensation relationships between them. Based on the compensation model, the influence of low frequency surface deformations on the system can be eliminated or partially eliminated. In this subsection, compensation of the off-axis TMA system with deformed PM (astigmatism) by adjusting SM is discussed.

To establish the relationships between the contribution of surface deformations and primary aberrations, Zernike polynomials are used. Here, the contribution of astigmatic deformation of PM can be regarded as the astigmatic component independent of the FOV, and the induced aberrations can be integrated into NAT [31]. In the proposed compensation model, the notation containing the astigmatism component is given by

$$\vec{\Psi}_{222}^{2} = W_{222}\vec{H}^{2} - 2\vec{H}\vec{A}_{222} + \vec{B}_{222}^{2}. \tag{20}$$

To integrate the astigmatism of PM into the compensation model of the perturbed off-axis system, it is necessary to add it directly to the existing astigmatic component that is independent of the FOV, given by

$$\vec{B}_{222}^{2} = {}_{M}\vec{B}_{222}^{2} + {}_{F}\vec{B}_{222}^{2}/B^{2}, \tag{21}$$

where ${}_{M}\vec{B}_{222}^{2}$ is a quadratic function of the aberration field decenter vectors and corresponds to the constant astigmatism induced by misalignments [31], ${}_{F}\vec{B}_{222}^{2}$ denotes the constant

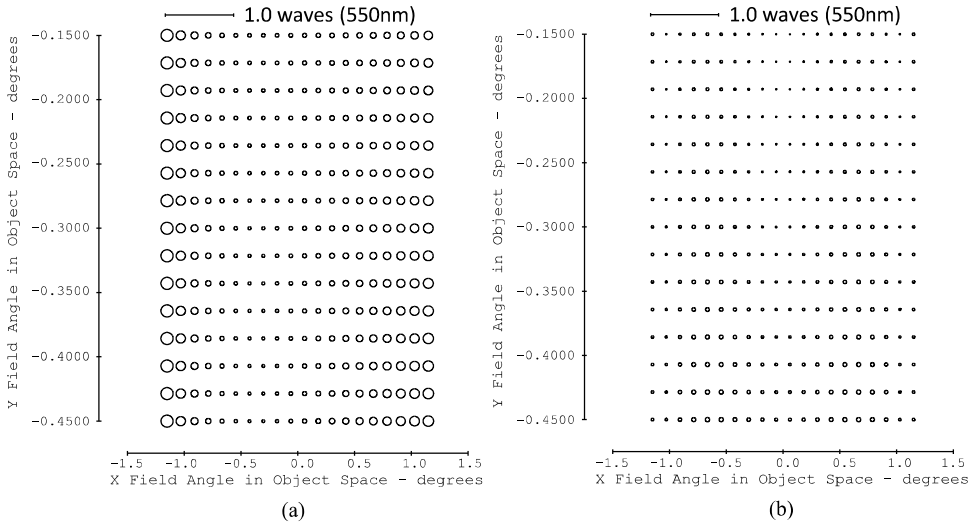

Fig. 4. Full field displays (FFDs) before and after compensating for the misaligned TM. (a) FFDs for RMS wavefront errors after misalignment (average value 0.088λ). (b) FFDs for RMS wavefront errors after compensation (average value 0.039λ).

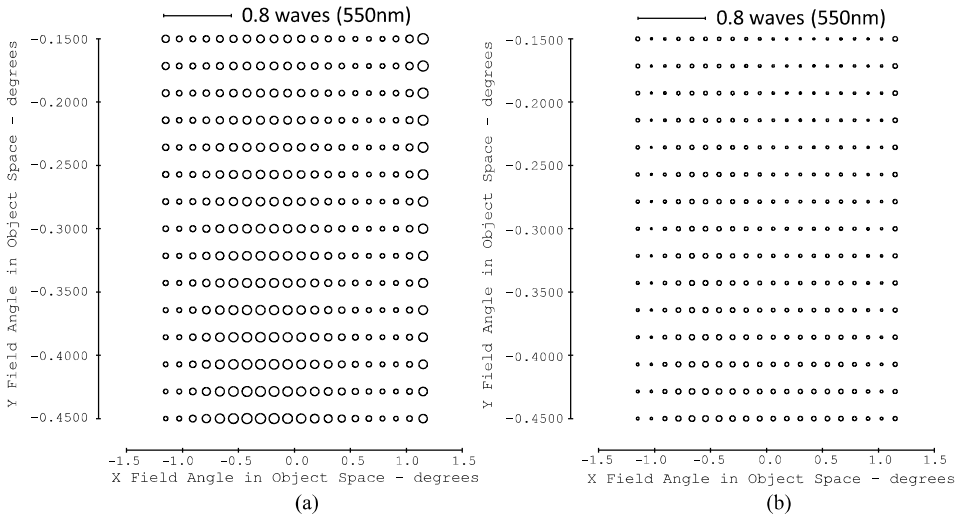

Fig. 5. Full field displays (FFDs) before and after compensating for the deformed PM. (a) FFDs for RMS wavefront errors after deformation (average value 0.083λ). (b) FFDs for RMS wavefront errors after compensation (average value 0.041λ).

Table 3. Introduced (I-V) Astigmatic Figure Errors of PM for the Off-Axis TMA Telescope[a]

	${}_F C_5^{\mathrm{PM}}$	${}_F C_6^{\mathrm{PM}}$
I-V	−0.08	0.05

[a]The fringe Zernike coefficients are in λ.

Table 4. Computed (C-V) and Referred (R-V) Compensation Values of SM and FP for the Off-Axis TMA Telescope with Deformed PM[a]

	$\mathrm{XDE_{SM}}$	$\mathrm{YDE_{SM}}$	$\mathrm{ADE_{SM}}$	$\mathrm{BDE_{SM}}$
C-V	−0.0916	−0.0941	0.0012	−0.0016
R-V	−0.0945	−0.0912	0.0013	−0.0015
	$\mathrm{ZDE_{FP}}$	$\mathrm{ADE_{FP}}$	$\mathrm{BDE_{FP}}$	
C-V	0.1123	−0.0357	−0.0076	
R-V	0.1135	−0.0346	−0.0078	

[a]XDE, YDE, and ZDE are in millimeters, ADE and BDE in degrees.

astigmatism induced by the astigmatic deformation of PM, and B denotes the ratio of the radius of the decentered pupil to that of the parent pupil. In other words, the aberration induced by deformation is included in $\vec{B}_{222}^{2}$, so it is introduced into the compensation model.

Here, the system used is the same as in the previous subsection, and the parameters used are also the same. The introduced astigmatic deformation of PM (${}_F C_5^{\mathrm{PM}}$ and ${}_F C_6^{\mathrm{PM}}$) for the off-axis TMA telescope is shown in Table 3. Similar to the case of misaligned TM, according to the proposed method, the aberration field decenter vectors of SM can be determined, and then the compensation values of SM for the deformed PM can be determined. The referred values can also be obtained by optical simulation software. The computed and referred compensation values of SM and FP for the deformed PM are listed in Table 4. It can be seen that the computed values based on the proposed method are very close to the referred values.

The computed compensation values are introduced into optical simulation software. The RMS wavefront errors before and after compensating for the deformed PM are characterized in Fig. 5. It can be seen that the RMS wavefront errors of the off-axis telescope with deformed PM can be compensated for satisfactorily. The average RMS wavefront error in the off-axis system is reduced from 0.083λ (after deformation) to 0.041λ (after compensation), which can well meet the system performance requirements.

The results indicate that the proposed method in this paper is effective. It should be noted that before compensating for the effect of astigmatic deformation of PM using the proposed method, the astigmatic deformation values need to be determined. According to the computation method for misalignments and surface figure errors, the perturbation values can be obtained with a certain period, and the perturbed systems can be compensated for based on the idea proposed in this paper. Although only the astigmatism compensation problem is discussed here, other surface deformation compensation problems can be solved by a similar method.

C. Monte Carlo Simulation

The ST method is usually used in engineering. To demonstrate the effectiveness of the proposed method, it is compared to the ST method. Monte Carlo simulations are performed to evaluate these two methods. Here, only the system compensation for misaligned TM is simulated, and similar results can be obtained in other situations.

Table 5. Introduced Four Different Cases of Misaligned TM Considered in Monte Carlo Analysis[a]

	$\mathrm{XDE_{TM}}$, $\mathrm{YDE_{TM}}$	$\mathrm{ADE_{TM}}$, $\mathrm{BDE_{TM}}$	ME
Case 1	[−0.2, 0.2]	[−0.015, 0.015]	\
Case 2	[−0.5, 0.5]	[−0.03, 0.03]	\
Case 3	[−0.8, 0.8]	[−0.05, 0.05]	\
Case 4	[−0.2, 0.2]	[−0.015, 0.015]	5%

[a]XDE and YDE are in millimeters; ME denotes the measurement error.

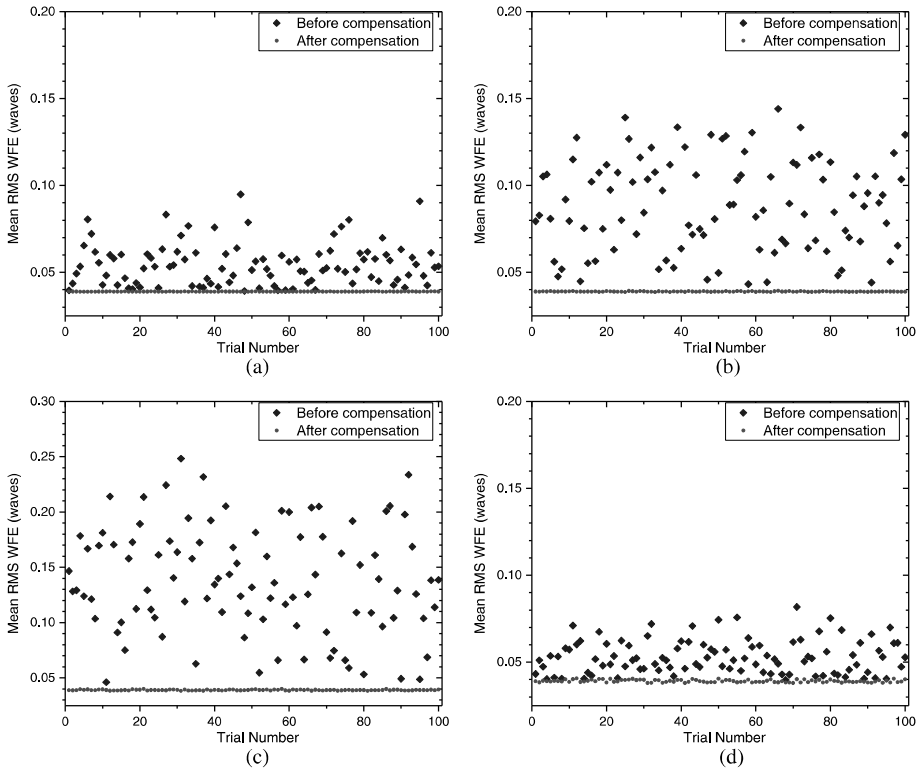

Fig. 6. System WFEs (average RMS) before and after compensation for misaligned TM of four cases using the proposed method. (a) WFEs for case 1, (b) WFEs for case 2, (c) WFEs for case 3, and (d) WFEs for case 4. Squares denote system WFEs (average RMS) before compensation. Dots denote system WFEs (average RMS) after compensation.

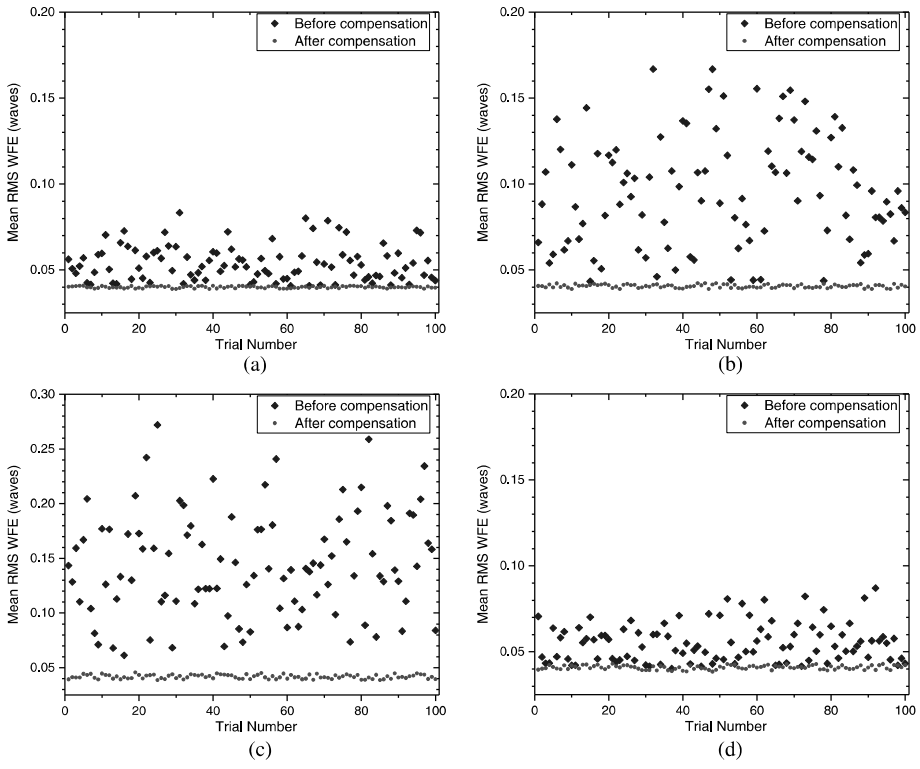

Fig. 7. System WFEs (average RMS) before and after compensation for misaligned TM of four cases using the ST method. (a) WFEs for case 1, (b) WFEs for case 2, (c) WFEs for case 3, and (d) WFEs for case 4. Squares denote system WFEs (average RMS) before compensation. Dots denote system WFEs (average RMS) after compensation.

Four different cases are adopted in the Monte Carlo simulations, which are listed in Table 5. In case 1, case 2, and case 3, the ranges increase in sequence without measurement errors. Case 4 includes 5% relative measurement error.

In the simulation, 100 trial perturbed states are randomly generated following a standard uniform distribution for each case. There are 400 pairs of misalignments for all cases, and the simulations for each trial system can be performed by using the proposed method and the ST method. The compensation values can be obtained for each perturbed state, and the computed values are used to compensate for the perturbed off-axis system. To evaluate the simulation results more fully, the average RMS wavefront errors (WFEs) can be obtained for each trial system. The average RMS WFEs before and after compensation for misaligned TM based on the proposed method and the ST method are shown in Figs. 6 and Fig. 7, respectively.

As can be seen in Fig. 6, the compensation results for case 1, case 2, and case 3 demonstrate the correctness of the proposed method. Comparing Fig. 6 with Fig. 7, it can be found that in cases 1–3, after compensation based on the proposed method, the off-axis system has better compensation performance. It indicates that the proposed method is basically not affected by the misalignment range. However, with the increase in perturbation range, the compensation performance of the ST method decreases (case 2 and case 3). As the perturbation range increases, the linear relationship in the ST method is broken, which can lead to degradation of system performance. A comparison of the results for case 4 shows the two methods are affected by measurement errors, but the proposed method is also better than the ST method at the considered level of measurement errors. It can be concluded that the compensation results of the proposed method are better than the ST method in the same perturbation cases. The proposed method is a better choice for active compensation for perturbed off-axis telescopes.

5. CONCLUSION

In this paper, the wave aberration function in an orthogonalized form for perturbed off-axis telescopes was derived in the framework of NAT by using RMS normalization. The Zernike description was related directly to the NAT expression. The orthogonalized form can eliminate the cross terms in the aberration function and define a balance among classical aberrations. The orthogonalized aberration function was applied to analytically describe the RMS wavefront error in perturbed off-axis telescopes. The square sum of the coefficients of the orthogonalized function yields the system wavefront variance. The active compensation problem of perturbed systems was formulated as an optimization model, which took the weighted square sum of RMS wavefront errors at the representative field points as the objective function. Then, the off-axis TMA telescope was taken as an example, and the system compensation results were given. After optimal compensation, the average RMS wavefront errors in the off-axis TMA telescope with misaligned TM and deformed PM were reduced to 0.039λ and 0.041λ, respectively. They can well meet the system performance requirements. Finally, Monte Carlo simulations of the proposed method and ST method were carried out, which demonstrated the correctness and accuracy of the proposed method.

This paper proposes a general compensation method using NAT for perturbed off-axis telescopes. Although only the deformations on the stop are discussed in the paper, the method can be extended to take into account the deformations on the surface away from the stop through the specific pupil footprint for each field point. The method proposed in this paper can be used for reference in active compensation for complex off-axis systems.

APPENDIX A

This appendix provides the definition of the notations ($\vec{\Psi}_{131}$, $\vec{\Psi}^2_{222}$, etc.) used in Eq. (7) in Section 2, as defined in Ref. [28]. The difference is that the symbol "Ψ" replaces the symbol "[]". They can be given by

$$
\begin{cases}
\vec{\Psi}_{131} = W_{131}\vec{H} - \vec{A}_{131}, \\
\Psi_{220M} = W_{220M}(\vec{H}\cdot\vec{H}) - 2\vec{H}\cdot\vec{A}_{220M} + B_{220M}, \\
\vec{\Psi}^2_{222} = W_{222}\vec{H}^2 - 2\vec{H}\vec{A}_{222} + \vec{B}^2_{222}, \\
\vec{\Psi}_{311} = W_{311}(\vec{H}\cdot\vec{H})\vec{H} - 2(\vec{H}\cdot\vec{A}_{311})\vec{H} + 2B_{311}\vec{H} - (\vec{H}\cdot\vec{H})\vec{A}_{311} + \vec{B}^2_{311}\vec{H}^* - \vec{C}_{311}, \\
\vec{\Psi}_{151} = W_{151}\vec{H} - \vec{A}_{151}, \\
\Psi_{240M} = W_{240M}(\vec{H}\cdot\vec{H}) - 2\vec{H}\cdot\vec{A}_{240M} + B_{240M}, \\
\vec{\Psi}^2_{242} = W_{242}\vec{H}^2 - 2\vec{H}\vec{A}_{242} + \vec{B}^2_{242}, \\
\vec{\Psi}_{331M} = W_{331M}(\vec{H}\cdot\vec{H})\vec{H} - 2(\vec{H}\cdot\vec{A}_{331M})\vec{H} + 2B_{331M}\vec{H} - (\vec{H}\cdot\vec{H})\vec{A}_{331M} + \vec{B}^2_{331M}\vec{H}^* - \vec{C}_{331M}, \\
\vec{\Psi}^3_{333} = W_{333}\vec{H}^3 - 3\vec{H}^2\vec{A}_{333} + 3\vec{H}\vec{B}^2_{333} - \vec{C}^3_{333}, \\
\Psi_{420M} = \begin{bmatrix} W_{420M}(\vec{H}\cdot\vec{H})(\vec{H}\cdot\vec{H}) - 4(\vec{H}\cdot\vec{H})(\vec{H}\cdot\vec{A}_{420M}) \\ +4B_{420M}(\vec{H}\cdot\vec{H}) + 2\vec{H}^2\cdot\vec{B}^2_{420M} - 4\vec{H}\cdot\vec{C}_{420M} + D_{420M} \end{bmatrix}, \\
\vec{\Psi}^2_{422} = \begin{bmatrix} W_{422}(\vec{H}\cdot\vec{H})\vec{H}^2 - 2(\vec{H}\cdot\vec{H})\vec{H}\vec{A}_{422} + 3(\vec{H}\cdot\vec{H})\vec{B}^2_{422} \\ -2(\vec{H}\cdot\vec{A}_{422})\vec{H}^2 - \vec{C}^3_{422}\vec{H}^* + 3B_{422}\vec{H}^2 - 3\vec{H}\vec{C}_{422} + \vec{D}^2_{422} \end{bmatrix}, \\
\vec{\Psi}_{511} = \begin{bmatrix} W_{511}(\vec{H}\cdot\vec{H})(\vec{H}\cdot\vec{H})\vec{H} - 4(\vec{H}\cdot\vec{H})(\vec{H}\cdot\vec{A}_{511})\vec{H} + 6B_{511}(\vec{H}\cdot\vec{H})\vec{H} \\ +2(\vec{H}^2\cdot\vec{B}^2_{511})\vec{H} - 4(\vec{H}\cdot\vec{C}_{511})\vec{H} + 3D_{511}\vec{H} - (\vec{H}\cdot\vec{H})(\vec{H}\cdot\vec{H})\vec{A}_{511} \\ +2(\vec{H}\cdot\vec{H})\vec{B}^2_{511}\vec{H}^* - 4(\vec{H}\cdot\vec{H})\vec{C}_{511} - \vec{H}^2\vec{C}^*_{511} + 2\vec{D}^2_{511}\vec{H}^* - \vec{E}_{511} \end{bmatrix},
\end{cases}
\tag{A1}
$$

where

$$\begin{cases} W_{klm} = \sum_j W_{klmj}, \quad \vec{A}_{klm} = \sum_j W_{klmj}\vec{\sigma}_j, \\ B_{klm} = \sum_j W_{klmj}(\vec{\sigma}_j \cdot \vec{\sigma}_j), \quad \vec{B}^2_{klm} = \sum_j W_{klmj}\vec{\sigma}_j^2, \\ \vec{C}_{klm} = \sum_j W_{klmj}(\vec{\sigma}_j \cdot \vec{\sigma}_j)\vec{\sigma}_j, \quad \vec{C}^3_{klm} = \sum_j W_{klmj}\vec{\sigma}_j^3, \\ D_{klm} = \sum_j W_{klmj}(\vec{\sigma}_j \cdot \vec{\sigma}_j)^2, \quad \vec{D}^2_{klm} = \sum_j W_{klmj}(\vec{\sigma}_j \cdot \vec{\sigma}_j)\vec{\sigma}_j^2, \\ \vec{E}_{klm} = \sum_j W_{klmj}(\vec{\sigma}_j \cdot \vec{\sigma}_j)^2\vec{\sigma}_j. \end{cases} \tag{A2}$$

Funding. National Natural Science Foundation of China (61705223, 61905241); National Key Research and Development Program of China (2016YFB0500100).

Disclosures. The authors declare no conflicts of interest.

REFERENCES

1. H. J. Juranek, R. Sand, J. Schweizer, B. Harnisch, B. Kunkel, E. Schmidt, A. Litzelmann, F. Schillke, and G. Dempewolf, "Off-axis telescopes: the future generation of Earth observation telescopes," Proc. SPIE **3439**, 104–115 (1998).
2. L. G. Cook, "Three-mirror anastigmat used off-axis in aperture and field," Proc. SPIE **183**, 207–211 (1979).
3. R. N. Wilson, "Active optics and the new technology telescope (NTT): the key to improved optical quality at lower cost in large astronomical telescopes," Contemp. Phys. **32**, 157–171 (1991).
4. M. Liang, V. Krabbendam, C. F. Claver, S. Chandrasekharan, and B. Xin, "Active optics in large synoptic survey telescope," Proc. SPIE **8444**, 84444Q (2012).
5. V. Costes, D. Laubier, P. Darre, and L. Perret, "Optical design and active optics for next generation space telescopes," Proc. SPIE **8860**, 88600B (2013).
6. J. M. Howard, "Optical modeling activities for NASA's James Webb space telescope (JWST): III. Wavefront aberrations due to alignment and figure compensation," Proc. SPIE **6675**, 667503 (2007).
7. J. M. Howard, K. Q. Ha, R. Shiri, J. S. Smith, G. Mosier, and D. Muheim, "Optical modeling activities for NASA's James Webb space telescope (JWST): V. Operational alignment updates," Proc. SPIE **7071**, 70710X (2008).
8. N. Devaney, C. Reinlein, N. Lange, M. Goy, A. Goncharov, and P. Hallibert, "HYPATIA and STOIC: an active optics system for a large space telescope," Proc. SPIE **9904**, 990469 (2016).
9. N. Devaney, F. Kenny, A. Goncharov, M. Goy, and C. Reinlein, "Development of a prototype active optics system for future space telescopes," Appl. Opt. **57**, E101–E106 (2018).
10. R. Upton, T. Rimmele, and R. Hubbard, "Active optical alignment of the advanced technology solar telescope," Proc. SPIE **6271**, 62710R (2006).
11. S. Kim, H. S. Yang, Y. W. Lee, and S. W. Kim, "Merit function regression method for efficient alignment control of two-mirror optical systems," Opt. Express **15**, 5059–5068 (2007).
12. R. V. Shack and K. P. Thompson, "Influence of alignment errors of a telescope system," Proc. SPIE **251**, 146–153 (1980).
13. K. Thompson, "Description of the third-order optical aberrations of near-circular pupil optical systems without symmetry," J. Opt. Soc. Am. A **22**, 1389–1401 (2005).
14. K. P. Thompson, T. Schmid, O. Cakmakci, and J. P. Rolland, "Real-ray-based method for locating individual surface aberration field centers in imaging optical systems without rotational symmetry," J. Opt. Soc. Am. A **26**, 1503–1517 (2009).
15. K. P. Thompson, "Multinodal fifth-order optical aberrations of optical systems without rotational symmetry: spherical aberration," J. Opt. Soc. Am. A **26**, 1090–1100 (2009).
16. K. P. Thompson, "Multinodal fifth-order optical aberrations of optical systems without rotational symmetry: the comatic aberrations," J. Opt. Soc. Am. A **27**, 1490–1504 (2010).
17. K. P. Thompson, "Multinodal fifth-order optical aberrations of optical systems without rotational symmetry: the astigmatic aberrations," J. Opt. Soc. Am. A **28**, 821–836 (2011).
18. K. P. Thompson, "The astigmatic aberration field in active primary mirror astronomical telescopes," Adv. Opt. Technol. **2**, 89–95 (2013).
19. G. Ju, C. Yan, Z. Gu, and H. Ma, "Computation of astigmatic and trefoil figure errors and misalignments for two-mirror telescopes using nodal-aberration theory," Appl. Opt. **55**, 3373–3386 (2016).
20. J. Sebag, W. Gressler, T. Schmid, J. P. Rolland, and K. P. Thompson, "LSST telescope alignment plan based on nodal aberration theory," Publ. Astron. Soc. Pac. **124**, 380–390 (2012).
21. X. Zhang, D. Zhang, S. Xu, and H. Ma, "Active optical alignment of off-axis telescopes based on nodal aberration theory," Opt. Express **24**, 26392–26413 (2016).
22. B. Jiang, S. Z. Zhou, K. Jiang, H. Y. Fu, and C. Mei, "Alignment off-axis optical system using nodal aberration theory," Proc. SPIE **8910**, 89100E (2013).
23. G. Ju, C. Yan, Z. Gu, and H. Ma, "Aberration fields of off-axis two mirror astronomical telescopes induced by lateral misalignments," Opt. Express **24**, 24665–24703 (2016).
24. X. Zhang, S. Xu, H. Ma, and N. Liu, "Optical compensation for the perturbed three mirror anastigmatic telescope based on nodal aberration theory," Opt. Express **25**, 12867–12883 (2017).
25. X. Bai, G. Ju, H. Ma, and S. Xu, "Aberrational interactions between axial and lateral misalignments in pupil-offset off-axis two-mirror astronomical telescopes," Appl. Opt. **58**, 7693–7707 (2019).
26. G. Ju, H. Ma, Z. Gu, and C. Yan, "Experimental study on the extension of nodal aberration theory to pupil-offset off-axis three-mirror anastigmatic telescopes," J. Astron. Telesc. Instrum. Syst. **5**, 029001 (2019).
27. R. A. Buchroeder, "Tilted component optical systems," Ph.D. dissertation (University of Arizona, 1976).
28. K. P. Thompson, K. Fuerschbach, and J. P. Rolland, "An analytic expression for the field dependence of FRINGE Zernike polynomial coefficients in optical systems that are rotationally nonsymmetric," Proc. SPIE **7849**, 784906 (2010).
29. R. J. Noll, "Zernike polynomials and atmospheric turbulence," J. Opt. Soc. Am. **66**, 207–211 (1976).
30. R. W. Gray and J. P. Rolland, "Wavefront aberration function in terms of R. V. Shack's vector product and Zernike polynomial vectors," J. Opt. Soc. Am. A **32**, 1836–1847 (2015).
31. T. Schmid, J. P. Rolland, A. Rakich, and K. P. Thompson, "Separation of the effects of astigmatic figure error from misalignments using nodal aberration theory (NAT)," Opt. Express **18**, 17433–17447 (2010).
32. Z. H. Zhan, J. Zhang, Y. Li, and H. S. Chung, "Adaptive particle swarm optimization," IEEE Trans. Syst. Man. Cybern. **39**, 1362–1381 (2009).